A Novel Subarray Digital Modulation Technique for Wideband Phased Array Radar

Zhennan Liang, Quanhua Liu, *Senior Member, IEEE*, and Teng Long, *Fellow, IEEE*

***Abstract*— A novel wideband digital array radar system is introduced in this article. The system has an open software-based processing architecture that provides a high degree of digitization and a flexible processing mode that employs digital stretch processing and digital modulation techniques to solve the beam divergence problem caused by the wide-angle scanning of both broadband and wideband array radar. The system simultaneously realizes a large range window, a wide dynamic range, and interpulse coherence for wideband array radar. The system is applicable not only to wideband linear frequency modulated (LFM) signals but also to wideband nonlinear frequency modulated (NLFM) signals. An engineering implementation scheme is also introduced. Key techniques, including wideband waveform generation, low data rate transmission, high-precision digitally modulated time-delay compensation, and high-precision system synchronization, are described in detail. In addition, an X-band experimental system is constructed, and the performance of this system is verified using typical target detection experiments.**

***Index Terms*— Array radar, digital modulation, digital stretch processing, digitization, dispersion effect, wideband radar.**

I. Introduction

IN COMBINING digital technology and array radar technology, digital array radar offers the advantages of multifunctionality, multiple beams, a wide dynamic range, and adaptive nulls [1]–[8]. To achieve target recognition in complex scenarios, digital array radar should have high resolution [9], [10], including a high range resolution and a high angular resolution. High-resolution radars utilize wideband signals to achieve high range resolution. The increased radar-signal bandwidth reduces the range resolution to below the target size. Targets can be distinguished and recognized precisely by providing high-resolution range profiles [11] with target feature information [12]–[15]. Therefore, the development of large-aperture digital array radar capable of a long range, high resolution, and wide-scan angle has received increasing attention.

According to the Nyquist sampling theorem, a high-speed analog-to-digital (A/D) converter is required for the undistorted sampling of wideband signals. This converter generates a considerable amount of raw data and places high demands on data transmission and real-time signal processing. Given prior information about a range window in which a target may exist, only this window needs to be detected. A technique known as stretch processing [16], [17] is usually applied to effectively reduce the signal sampling rate, the amount of raw data for the range window of interest, and the burden of data transmission and real-time signal processing. Conventional array radar uses a distributed receiver with multiple receiving channels to perform stretch processing in the analog domain, thereby lowering the requirements for A/D converters. However, analog stretch processing needs to locally generate and distribute stretch processing reference signals to all of the receiving paths through a power divider. The distributed signals tend to have different magnitude–phase characteristics, which leads to amplitude–phase distortion of the wideband signal that seriously affects radar performance. Adaptive waveform distortion correction methods have been proposed in which an adaptive filter is used to suppress distortion [18], [19]. However, because distortion correction is performed in the time domain, performance is good around the center of the range window but deteriorates for a target that is more remote from the scene center. Thus, a conventional wideband radar system is only effective for a small range window, and the radar performance deteriorates as the size of the range window increases [20], [21].

With the development of hardware technology, high-speed A/D converters are no longer a technical bottleneck. Therefore, the digitization stage can be moved closer to the antenna, allowing distortions in the radar front end to be measured and calibrated [22]. This improvement not only decreases amplitude–phase distortion from signal propagation in the analog domain but also provides an accurate correction of the distortion in the frequency domain. Thus, a digital wideband radar system can correct the distorted echo signals from targets at any position in the range window [23]. That is, the digital wideband radar system can function effectively for a large range window.

In addition, there is an inherent contradiction between the signal bandwidth of large-aperture array radars and the electrical scanning capability of the beam, which manifests as the dispersion effect [24]. The beam shifts when scanning at wide bandwidths and large angles, resulting in an energy loss in the synthesized echo signal and a decrease in the detection ability of the radar. To prevent dispersion losses, an analog delay unit (ADU) is conventionally used to control

Manuscript received August 26, 2019; revised February 15, 2020; accepted March 21, 2020. Date of publication March 30, 2020; date of current version September 15, 2020. This work was supported by the National Natural Science Foundation of China under Grant 61771050, Grant 31727901, and Grant 61625103. The Associate Editor coordinating the review process was Yuri Alvarez Lopez. *(Corresponding author: Quanhua Liu.)*

The authors are with the School of Information and Electronics, Beijing Institute of Technology, Beijing 100081, China, and also with the Key Laboratory of Electronic and Information Technology in Satellite Navigation, Ministry of Education, Beijing 100081, China (e-mail: pumpkin_xixi@163.com; liuquanhua@bit.edu.cn; longteng@bit.edu.cn).

Color versions of one or more of the figures in this article are available online at http://ieeexplore.ieee.org.

Digital Object Identifier 10.1109/TIM.2020.2984417

the beam pointing at the subarray level [25]. That is, a phase shifter is applied in a subarray for beam control, and a proper intersubarray connection time-delay unit (TDU) is selected based on the beam pointing to control the beam. This method can reduce dispersion loss to a certain extent. However, an ADU can provide only a fixed delay, and quantization errors restrict the precision of the beam pointing control. Additional disadvantages associated with the ADU are high system complexity, large equipment, temperature sensitivity, and severe amplitude–phase distortion. For wideband digital array radar, a digital delay beam control method should be considered to achieve wideband digital beamforming in the digital domain and to effectively suppress dispersion loss [26]–[32]. In [26], a digital beamforming method was proposed based on an instantaneous wideband linear frequency modulated (LFM) signal, in which the beam divergence is compensated for through two time delays. In [27] and [28], a fractional delay filter was designed to accurately control the time delay. Based on this, a wideband digital transmitting beamformer was designed in [29] with a multiphase structure consisting of a direct digital synthesizer (DDS) and a fractional delay filter to generate and delay compensate for the transmitted signal. In [30], a method of delay compensation for the wideband digital receiving path was proposed that flexibly and digitally generates local oscillation signals to accurately compensate for the delay and phase of the receiving path. A wideband digital array test platform that generates wideband digital beams was built by using the adaptive beamforming algorithm in [31] and [32].

In summary, a novel wideband digital array radar architecture is proposed in this article, building on breakthroughs in key techniques, such as wideband digital waveform generation, digital stretch processing, high-precision digitally modulated time-delay compensation, and high-precision system synchronization. The transmission path generates wideband signals through direct digital synthesis, and a digital modulation technique is used to form the transmitted beams. The receiving path performs stretch processing in the digital domain and accurately compensates for the delay using subarray digital modulation to control the received beam pointing. The problems of mass data transmission of wideband array radar and beam divergence from wide-angle scanning are, thus, solved while achieving wideband array radar with a large range window, a wide dynamic range, and interpulse coherence. Based on this, an engineering implementation scheme is proposed, a prototype is built, and the performance of the novel system is verified experimentally.

The remainder of this article is organized as follows. In Section II, the novel wideband digital array radar system is introduced, and the advantages and characteristics of the system are elaborated. In Section III, the principles of the digital signal processing algorithm under the architecture of the novel system are described. In Section IV, the engineering implementation scheme of the system is designed, and key technical breakthroughs in engineering practice are described in detail. In Section V, a prototype is developed, and the performance of the wideband digital array radar is verified experimentally. Finally, conclusions are drawn in Section VI.

from the array.

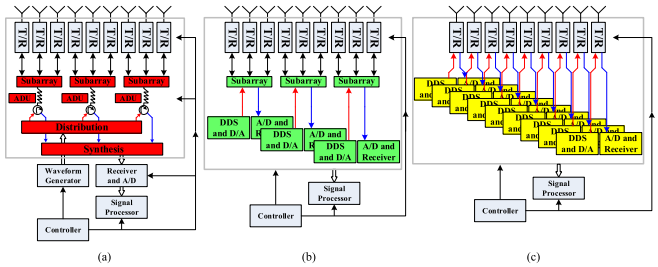

Fig. 1. Three generic wideband array radar system architectures with digitization. (a) Analog active phased arrays. (b) Subarray-level digital arrays. (c) Element-level digital arrays.

II. Novel Wideband Digital Array System

The architecture that is generally used in the current wideband array radar is shown in Fig. 1(a). To reduce the system cost and the computational burden, the radiating elements are grouped by subarray partitioning to reduce the number of paths, and signal processing is conducted at the subarray level to effectively reduce the system complexity. The delay is compensated for by using an ADU at the subarray level, reducing dispersion loss to a certain extent. Wideband transmission signals and wideband reference signals are then generated in the analog domain. The signal sampling rate is effectively reduced via analog stretch processing. The signal is then sampled with a low-speed A/D converter, and subsequent signal processing is conducted in the digital domain. As mentioned earlier, the performance issues of ADUs and analog stretch processing limit the improvement in the digital-based system performance because the digitization stage occurs far from the array.

There are two categories of digital array systems: subarray-level digital arrays and element-level digital arrays. A subarray-level digital array [see Fig. 1(b)] processes signals at the subarray level, moves the digitization stage forward, uses a high-speed A/D converter to generate wideband transmission signals and wideband reference signals in the digital domain, applies digital modulation to replace the ADU to accurately compensate for the subarray delay, and applies digital stretch processing instead of analog stretch processing to effectively reduce the signal sampling rate. This system can prevent many of the problems associated with the analog processing mode and fully exploits the high compensation accuracy and flexibility of digital processing. In addition, the signal processing at the subarray level is adequate for engineering applications. Element-level digital arrays [see Fig. 1(c)] process signals at the element level, move the digitization stage forward to the position closest to the array without a phase shifter, and control the array beam pointing via digital beamforming, maximizing the degrees of freedom of the array and the improvement in digital-based system performance. However, the element-level processing and subsequent beamforming are digital, and the existing hardware system cannot handle the potential mass data transmission and real-time processing.

A novel architecture for wideband digital array radar is shown in Fig. 2.

The upconverters and the downconverters shift the frequency spectrum of the wideband signals between intermediate frequency (IF) signals and radio frequency (RF) signals.

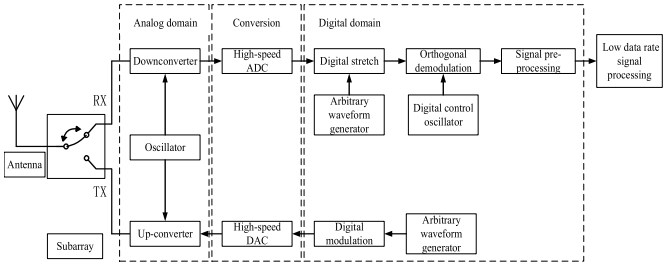

Fig. 2. Novel architecture for wideband digital array radar.

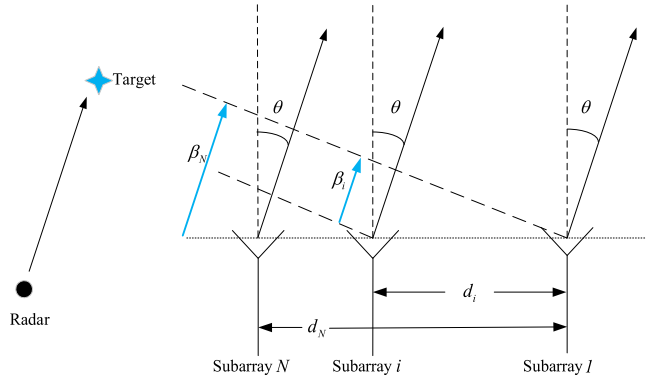

Fig. 3. Schematic of antenna array transmitting paths.

A high-speed A/D and D/A converter performs digital-to-analog or A/D conversion of wideband signals directly. The digital-domain signal processing includes transmitting and receiving path signal processing. For the transmitting path, a high-speed DDS is directly applied to generate the wideband signal. Digital modulation is then applied to precisely compensate for the time delay between the subarrays of the transmitting path. With the aid of digital stretch processing, the signal sampling rate is effectively reduced to conform to the signal transmission and real-time processing requirements of the receiving path. A digital control oscillator can flexibly produce two-way orthogonal local oscillation signals and compensate for the differences in the time delay and phase between the subarray paths by flexibly adjusting the local oscillation signal frequency and phase via digital orthogonal demodulation of the signals. A high-resolution range profile is obtained by signal preprocessing, and the time-delay difference between the subarray paths is ultimately compensated.

Compared with the conventional system architecture, the novel subarray-level digital array offers the following advantages.

1) An open software processing architecture, a high degree of digitization, and flexible processing.

2) *Wide Dynamic Range:* The digital radar provides the additional potential for improving the dynamic range by moving the digital stage close to the array face.

3) A large range window that is realized by compensating for systematic amplitude and phase distortions and other nonideal factors in the digital domain.

4) *Interpulse Coherence:* The subarray-level direct sample processing can fix the sampling trigger time in the coherence processing period, and a digitally stretched local oscillation can be produced from the coherence, preventing interpulse incoherence from the randomness triggered by local oscillations and realizing multipulse coherence processing.

5) *Anti-Interference:* Adaptive beamforming is applied to form the null of the antenna pattern to reject sidelobe jamming [31].

III. Wideband Digital Array Signal Processing

A. Transmitting Path

We consider an arbitrary wideband RF waveform $s_{\mathrm{RF}}(t)$

$$s_{\mathrm{RF}}(t) = \mathrm{rect}\left(\frac{t}{T}\right)\cos(2\pi(f_c t + \phi_s(t))) \tag{1}$$

where $\mathrm{rect}(\cdot)$ is a rectangular function with pulse duration T, f_c is the radar center frequency, and $\phi_s(t)$ represents a phase function that may or may not be quadratic.

The transmitted waveform is obtained by mixing the IF signal $s_{\mathrm{IF}}(t)$ with the local oscillator $s_{\mathrm{LO}}(t)$ and filtering. The center frequency of the IF waveform is denoted by f_{IF}

$$\begin{aligned} s_{\mathrm{IF}}(t) &= \mathrm{rect}\left(\frac{t}{T}\right)\cos(2\pi(f_{\mathrm{IF}}t + \phi_s(t))) \\ s_{\mathrm{LO}}(t) &= \cos(2\pi(f_c - f_{\mathrm{IF}})t). \end{aligned} \tag{2}$$

When the array radar radiates energy along a specific direction, the array configuration results in the signals transmitted by each subarray channel taking different paths to the same spatial position, as shown in Fig. 3.

To ensure the spatial superposition of all of the energies, a series of transmitted waveforms should be generated with different delays along the direction of the radar light of sight (LOS). Taking the first subarray as the reference unit, the transmitted waveform of the ith subarray is

$$s_{\mathrm{RF}\_i}(t) = \mathrm{rect}\left(\frac{t-\beta_i}{T}\right)\cos(2\pi(f_c(t-\beta_i) + \phi_s(t-\beta_i))) \tag{3}$$

where β_i is the additional time delay from the reference subarray to the ith subarray.

Thus, the transmitted IF waveform $s_{\mathrm{IF}\_i}(t)$ of the ith subarray is

$$\begin{aligned} s_{\mathrm{IF}\_i}(t) = \mathrm{rect}&\left(\frac{t-\beta_i}{T}\right) \\ &\cdot \cos(2\pi(f_{\mathrm{IF}}(t-\beta_i) + \phi_s(t-\beta_i) - (f_c - f_{\mathrm{IF}})\beta_i)). \end{aligned} \tag{4}$$

$s_{\mathrm{RF}\_i}(t)$ is obtained after mixing $s_{\mathrm{IF}\_i}(t)$ and $s_{\mathrm{LO}}(t)$ and bandpass filtering. As $\beta_i \ll T$, the envelope-term coefficient can be neglected to digitally generate the transmitted IF waveform

$$s_{\mathrm{IF}\_i}(t) = \cos(2\pi(f_{\mathrm{IF}}(t-\beta_i) + \phi_s(t-\beta_i) - (f_c - f_{\mathrm{IF}})\beta_i)). \tag{5}$$

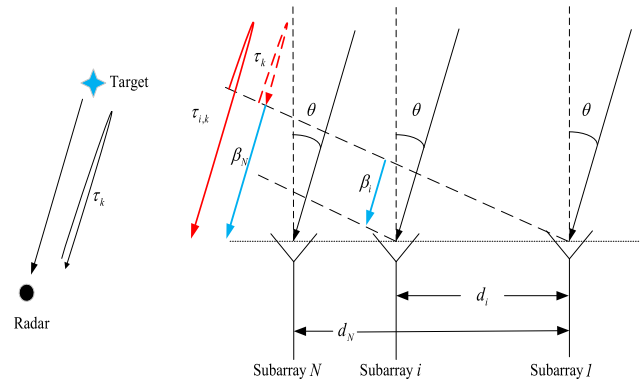

Fig. 4. Schematic of antenna array receiving paths.

B. Receiving Path

The target scatterer model of the wideband waveform is used in this article. Assume that the target is located on the LOS in the far-field and that the incident wave is a plane wave. Thus, the ideal noise-free received waveform can be written as

$$r_{\mathrm{RF}}(t) = \sum_{k=1}^{K} A_k s_{\mathrm{RF}}(t - \tau_k) \tag{6}$$

where K is the number of scatterers, A_k is the scattering amplitude coefficient of the kth scatterer, and τ_k is the time delay from the kth scatterer to the radar phase center.

The array configuration results in different transmitting paths that radiate to all of the subarray channels from the same spatial position. Fig. 4 shows a schematic of the antenna array receiving paths.

The number of the subarray channels is denoted by $i = 1, 2, \ldots, N$. The time delay of the target echo wave signal received by the ith subarray is $\tau_{i,k} = \tau_k + \beta_i$, where τ_k is the time delay from the kth scatterer to the radar phase center. The ideal noise-free echo can be expressed as

$$r_{\mathrm{RF}\_i}(t) = \sum_{k=1}^{K} A_k s_{\mathrm{RF}}(t - \tau_{i,k}). \tag{7}$$

1) Digital Stretch Processing: After mixing the echo $r_{\mathrm{RF}\_i}(t)$ with $s_{\mathrm{LO}}(t)$ and filtering, the IF echo can be written as

$$r_{\mathrm{IF}\_i}(t) = \sum_{k=1}^{K} \mathrm{rect}\left(\frac{t - \tau_{i,k}}{T}\right) A_k \cos(2\pi(f_{\mathrm{IF}} t + \phi_s(t - \tau_{i,k}) - f_c \tau_{i,k})) \tag{8}$$

where f_{IF} is the center frequency of the first IF waveform. The high-speed A/D converter samples the echo at a high speed and a sampling frequency f_s. Applying integer sampling units, the discrete form of (8) can be given as

$$r_{\mathrm{IF}\_i}(n) = \sum_{k=1}^{K} \mathrm{rect}\left(\left(\frac{n}{f_s} - \tau_{i,k}\right)/T\right) \cdot A_k \cos\left(2\pi\left(f_{\mathrm{IF}} \cdot \frac{n}{f_s} + \phi_s\left(\frac{n}{f_s} - \tau_{i,k}\right) - f_c \tau_{i,k}\right)\right). \tag{9}$$

The speed of an A/D converter increases to accommodate wider bandwidth waveforms, thereby generating a large amount of data. Stretch processing can be used to overcome this problem [17]. The echo $r_{\mathrm{IF}\_i}(n)$ received by the ith subarray and the reference waveform $r_{\mathrm{ref}}(n)$ generated by the waveform generator are mixed to significantly reduce the sampling rate and the data size. The reference signal is written as

$$r_{\mathrm{ref}}(n) = \mathrm{rect}\left(\left(\frac{n}{f_s} - \tau_0\right)/T_{\mathrm{ref}}\right) \cdot \cos\left(2\pi\left((f_{\mathrm{IF}} - f_L)\left(\frac{n}{f_s} - \tau_0\right) + \phi_s\left(\frac{n}{f_s} - \tau_0\right)\right)\right) \tag{10}$$

where f_L is the center frequency of the second IF waveform, T_{ref} is the duration of the reference signal, which is generally slightly larger than the transmitted pulsewidth, and τ_0 is the time delay of the reference signal that is set based on prior information about the target position to ensure that the reference signal can cover the transmitted signal.

Neglecting the envelope term, the stretch processing results can be written as

$$d_i(n) = r_i(n) r_{\mathrm{ref}}(n) = \sum_{k=1}^{K} A_k \cdot \cos\left(2\pi\left(\begin{array}{l} f_L \frac{n}{f_s} + \phi_s\left(\frac{n}{f_s} - \tau_{i,k}\right) \\ -\phi_s\left(\frac{n}{f_s} - \tau_0\right) + \varphi(\tau_{i,k}, \tau_0)\end{array}\right)\right). \tag{11}$$

The phase term is written as

$$\varphi(\tau_{i,k}, \tau_0) = (f_{\mathrm{IF}} - f_L)\tau_0 - f_c \tau_{i,k}. \tag{12}$$

The left-hand side of (11) changes slowly over time because $\phi_s((n/f_s) - \tau_0)$ is subtracted from the phase $\phi_s((n/f_s) - \tau_{i,k})$. Therefore, $d_i(n)$ in (11) will generally have a narrower bandwidth than $r_i(t)$ in (7), thereby lowering the required sampling rate.

The wideband waveform is stretched by the procedure above. Next, the IF signal shown in (11) is demodulated to the baseband by digital orthogonal demodulation.

2) Digital Orthogonal Demodulation: To apply digital signal processing, orthogonal demodulation is generally required to produce a two-way local oscillation signal, which can be written as

$$\begin{aligned} U_I(n) &= \cos\left(2\pi f_L \frac{n}{f_s} + \varphi\right) \\ U_Q(n) &= \sin\left(2\pi f_L \frac{n}{f_s} + \varphi\right). \end{aligned} \tag{13}$$

The waveform $d_i(n)$ that is obtained after digital stretch processing is mixed with the two-way local oscillation signal and subjected to low-pass filtering to produce the following complex signal:

$$p_i(n) = \sum_{k=1}^{K} A_k \cdot \exp\left(j2\pi\left(\phi_s\left(\frac{n}{f_s} - \tau_{i,k}\right) - \phi_s\left(\frac{n}{f_s} - \tau_0\right) + \varphi(\tau_{i,k}, \tau_0) - \varphi\right)\right). \tag{14}$$

The two-way local oscillation signal is generated by the digital control oscillator. Therefore, the time delay and phase differences between the received waveform of the subarrays can be compensated for by adjusting the frequency and phase of the two-way local oscillation signal.

The variable subarray number i is eliminated to compensate for the third term $\varphi(\tau_{i,k}, \tau_0)$ in (14). The one-way local oscillation signal generated by the digital control oscillator is expressed as

$$U_I(n) = \cos\left(2\pi f_L \frac{n}{f_s} - f_c\beta_i\right)$$
$$U_Q(n) = \sin\left(2\pi f_L \frac{n}{f_s} - f_c\beta_i\right). \tag{15}$$

After mixing and low-pass filtering, the complex waveform can be written as

$$p_i(n) = \sum_{k=1}^{K} A_k \cdot \exp\left(j2\pi\left(\phi_s\left(\frac{n}{f_s} - \tau_{i,k}\right) - \phi_s\left(\frac{n}{f_s} - \tau_0\right) + \varphi(\tau_k, \tau_0)\right)\right) \tag{16}$$

where the phase deviation is expressed as

$$\varphi(\tau_k, \tau_0) = (f_{\mathrm{IF}} - f_L)\tau_0 - f_c\tau_k. \tag{17}$$

The absence of the subarray number i in the equation indicates the compensation of the third term $\varphi(\tau_{i,k}, \tau_0)$ by orthogonal demodulation. However, the time-delay compensation for the first term $\phi_s(\frac{n}{f_s} - \tau_{i,k})$ in (14) must be treated further by signal preprocessing.

3) Signal Preprocessing: A matched filter is obtained by correlating a known delayed signal with an unknown signal. This is equivalent to convolving the unknown signal with a conjugated time-reversed version of the known delayed signal [17]. Therefore, a series of proper standard receiving waveforms $\psi_i(n, \tau)$ are built for each subarray to compensate for the time-delay difference between the subarrays. The standard receiving waveform corresponding to subarray number i is assumed to be

$$\psi_i(n, \tau) = \exp\left(j2\pi\left(\phi_s\left(\frac{n}{f_s} - \tau_0\right) - \phi_s\left(\frac{n}{f_s} - \tau - \beta_i\right)\right)\right). \tag{18}$$

The high-resolution range profile $P_i(\tau)$ can be obtained by projecting the low data rate signal $p_i(n)$ onto the standard receiving waveform $\psi_i(n, \tau)$, where the peak position is the target position and is mathematically expressed as

$$\begin{aligned} P_i(\tau) &= |\langle p_i(n), \psi_i(n, \tau)\rangle| \\ &= \left|\sum_{n=\tau_0}^{\tau_0+T_{\mathrm{ref}}} \sum_{k=1}^{K} A_k \exp\left(j2\pi\left(\phi_s\left(\frac{n}{f_s} - \tau_{i,k}\right) - \phi_s\left(\frac{n}{f_s} - \tau_0\right) + \varphi(\tau_k, \tau_0)\right)\right)\right. \\ &\quad \left.\times \exp\left(-j2\pi\left(\phi_s\left(\frac{n}{f_s} - \tau - \beta_i\right) - \phi_s\left(\frac{n}{f_s} - \tau_0\right)\right)\right)\right| \\ &= \left|\sum_{k=1}^{K} A_k \exp(j2\pi\varphi(\tau_k, \tau_0)) \sum_{n=\tau_0}^{\tau_0+T_{\mathrm{ref}}} \exp\left(j2\pi\phi_s\left(\frac{n}{f_s} - \tau_{i,k}\right)\right)\right. \\ &\quad \left.\times \exp\left(-j2\pi\phi_s\left(\frac{n}{f_s} - \tau - \beta_i\right)\right)\right| \\ &= \left|\sum_{k=1}^{K} A_k \sum_{n=\tau_0}^{\tau_0+T_{\mathrm{ref}}} s(n - \tau_{i,k})s^*(n - \tau - \beta_i)\right| \\ &= \left|\sum_{k=1}^{K} A_k \sum_{n=\tau_0}^{\tau_0+T_{\mathrm{ref}}} s(n - \tau_k - \beta_i)s^*(n - \tau - \beta_i)\right| \\ &= 9\left|\sum_{k=1}^{K} A_k \underbrace{\sum_{n'=\tau_0+\beta_i}^{\tau_0+T_{\mathrm{ref}}+\beta_i} s(n' - \tau_k)s^*(n' - \tau)}_{R(\tau-\tau_k)}\right| \end{aligned} \tag{19}$$

where the expression $R(\tau - \tau_k)$ represents the τ_k-shifted autocorrelation $R(\tau)$ of the emitted waveform $s(t)$. Thus, for a preset range window $[\tau_0, \tau_0 + T_{\mathrm{ref}}]$, the algorithm proposed above produces a range profile $P_i(\tau)$ over the desired range window that is, in fact, equivalent to that produced by conventional matched filtering. Moreover, the signal preprocessing result has not been associated with the subarray number i. Thus, coherence synthesis can be achieved for the entire range profile.

So far, the wideband signals have been subjected to digital stretch processing, orthogonal demodulation, and signal preprocessing in the digital domain and precisely compensated for the time delay of each subarray path. The obtained high-resolution range profile can be used to estimate the target parameter. In this article, the signal type is arbitrary. Hence, the processing algorithm is applicable to LFM and other chirp-like nonlinear frequency modulated (NLFM) waveforms [35], [36].

IV. Engineering Application of Wideband Digital Array

Based on the analysis provided in Section III, an engineering implementation scheme for a wideband phased array radar based on an LFM signal is proposed in this section. Digital waveform generation, digital stretch processing, high-precision time-delay compensation, and high-precision system synchronization are presented in detail.

A. Transmitting Path

According to the analysis in Section III, a time delay is needed for signals with different subarray paths to compensate for the difference in the wave paths from the antenna beam pointing and to ensure that the transmitted signals of all of the antennae are simultaneously superposed in phase at the space target. Hence, all of the subarray paths generate the required wideband signals in the digital domain according to (5).

The direct digital chirp synthesis (DDCS) algorithm is an emerging digital signal generation method [33]. This method has a simple circuit structure with a high integration level and

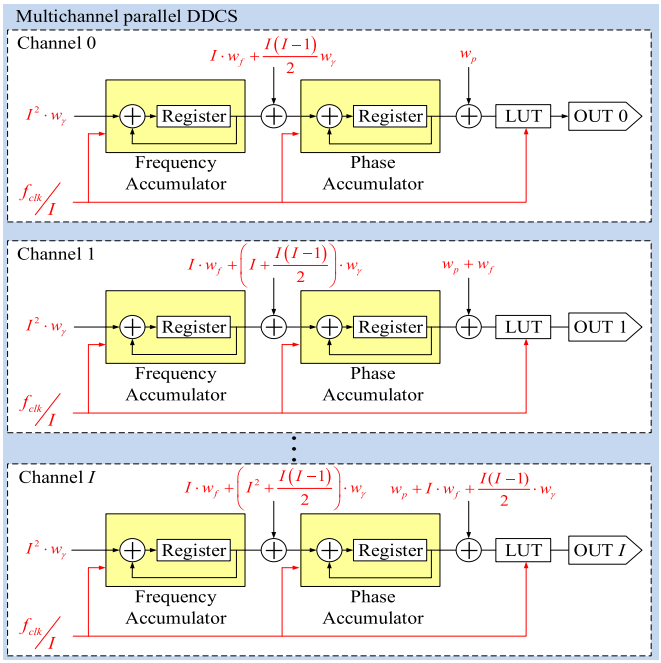

Fig. 5. Diagram of multichannel parallel DDCS.

fine flexibility. This algorithm can adjust the signal bandwidth, the pulsewidth, and the center frequency in real time. However, while the sampling frequency of a D/A converter usually exceeds 1 GHz to satisfy the direct sampling of wideband signals, the operating clock frequency of a field-programmable gate array (FPGA) usually ranges from 100 to 300 MHz. Therefore, samples are often generated in parallel to keep up with the D/A converter sample rates [33], [34].

1) Multichannel Parallel Versatile Waveform Generator: A DDCS consists of a frequency accumulator (FA), a phase accumulator (PA), a lookup table (LUT) that stores the values of sine signals, a D/A converter, and a low-pass filter. The required signals can be generated by dynamically adjusting three parameters, namely, the chirp rate control word w_γ, the frequency control word w_f, and the phase control word w_p. The output phase at the nth moment in time is

$$\theta(n) = \frac{w_\gamma}{2}n^2 + \left(w_f - \frac{w_\gamma}{2}\right)n + w_p. \tag{20}$$

According to the output phase expression of the LFM signal, the conversion relationships among the starting frequency f_0, the chirp rate γ, the chirp rate control word w_γ, and the frequency control word w_f are given by

$$\begin{aligned} w_\gamma &= \frac{\gamma}{2^N} \times f_{\text{clk}}^2 \\ w_f &= \frac{f_0}{2^N} \times f_{\text{clk}} + \frac{w_\gamma}{2} \end{aligned} \tag{21}$$

where f_{clk} is the working frequency of the DDCS waveform generator and N is the word length of the accumulator.

A multichannel parallel DDCS waveform generator is designed, as shown in Fig. 5, to meet the requirements of engineering applications. The number of parallel channels is denoted by I, and the operating frequency is reduced to (f_{clk}/I). The DDCS parameters of each channel need to be precisely designed. Substituting $n = mI + i (m = 0, 1, 2, \ldots, i = 0, 1, \ldots I-1)$ into (20) yields

$$\begin{aligned} \theta(mI+i) &= \frac{w_\gamma}{2}(mI+i)^2 + \left(w_f - \frac{w_\gamma}{2}\right)\cdot(mI+i) + w_p \\ &= \frac{w'_\gamma}{2}m^2 + \left(w'_f - \frac{w'_\gamma}{2}\right)m + w'_p. \end{aligned} \tag{22}$$

The calculation equations of the parameters for the ith channel are

$$\begin{aligned} w'_\gamma &= I^2 w_\gamma \\ w'_f &= I w_f + \left(iI + \frac{I(I-1)}{2}\right)w_\gamma \\ w'_p &= w_p + i w_f + \frac{i(i-1)}{2}w_\gamma. \end{aligned} \tag{23}$$

The DDCS control parameter of each channel can be accurately calculated using (21) and (23). Digital technologies offer greater flexibility for generating diverse bandwidth LFM waveforms.

2) Implementation of Transmitted Beamforming by Digital Modulation: For wideband phased array radar, a digital technique is applied to generate the wideband waveform, which is called a digital waveform. A flexible and controllable signal waveform can meet the demands of the various radar work patterns. More importantly, the digital technique can realize a flexible and controllable digital delay.

For an LFM signal, substituting the time phase function $\phi_s(t) = (1/2)\gamma t^2$ into (5) yields

$$\begin{aligned} s_{\text{IF\_}i}(t) &= \exp\left(j2\pi\left(f_{\text{IF}}(t-\beta_i) + \frac{1}{2}\gamma(t-\beta_i)^2 - (f_c - f_{\text{IF}})\beta_i\right)\right) \\ &= \exp\left(j2\pi\left((f_{\text{IF}} - \gamma\beta_i)t + \frac{1}{2}\gamma t^2 + \frac{1}{2}\gamma\beta_i^2 - f_c\beta_i\right)\right). \end{aligned} \tag{24}$$

Apparently, the time delay turns into an initial frequency term for the LFM signal and an initial phase term for the wideband signal. Therefore, each transmitted channel can flexibly realize a digital delay through the precise control of the starting frequency term and the phase of the transmitted signal.

As shown in Fig. 6, each channel corresponds to an independent multichannel parallel DDCS module for which the starting frequency and phase can be separately controlled. The module can also generate a corresponding wideband signal according to the equation. Therefore, the flexible digital delay can be realized for different channels to achieve transmitted beamforming.

In (24), the time delays of different channels are compensated for using digital modulation. The accuracy of the time-delay compensation is related to the frequency and phase resolution of the wideband signal, that is, the higher the frequency and phase resolution, the higher the accuracy of the time-delay compensation.

B. Receiving Path

1) Digital Stretch Processing: A digital stretch processing diagram is shown in Fig. 7. The mixing, filtering, and decimation of the signal and reference signal are performed by means

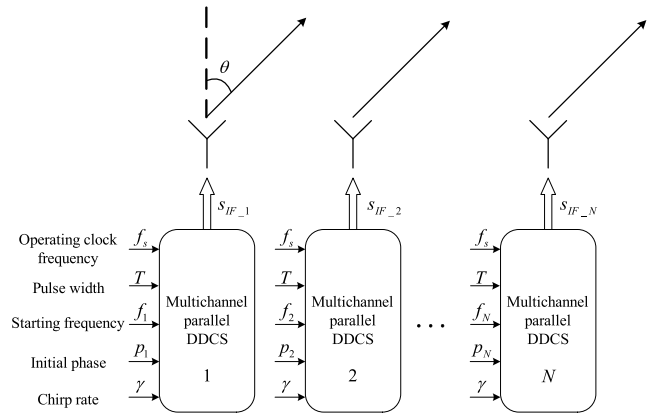

Fig. 6. Implementation of transmitted beamforming by digital modulation.

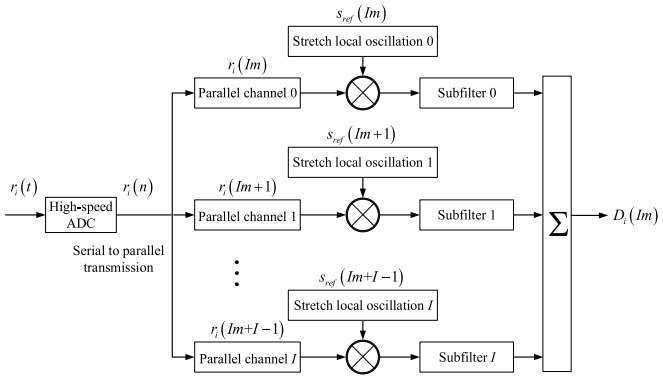

Fig. 7. Diagram of subarray digital stretch processing.

of multichannel parallel processing. The key problem solved in the process is the mismatch between the operating clocks of the high-speed A/D converter and the FPGA hardware.

The stretch processing reference signal is generated by a multichannel parallel versatile waveform generator, which is not described in detail here. The additional delay of the reference signal that can be measured and compensated is only related to the range accuracy. Without loss of generality, we assume that the additional delay of reference is zero. After the mixing processing of the received wideband signal and the stretch processing reference signal, the high-frequency component must be filtered by a low-pass filter. In addition, stretch processing of the wideband significantly decreases the signal bandwidth. Decimation processing is commonly adopted to reduce the signal sampling rate to ease the burden of signal transmission and signal processing. Therefore, we design a multiphase decimation filter that hides the decimation operation in the filtering process and reduces the sampling rate of the output signal while performing low-pass filtering.

2) Implementation of Receiving Beamforming by Digital Modulation: For an LFM signal, substituting the time phase function $\phi_s(t) = (1/2)\gamma t^2$ into (19) yields

$$\begin{aligned} P_i(\tau) &= |\langle p_i(n), \psi_i(n,\tau)\rangle| \\ &= \left| \sum_{n=\tau_0}^{\tau_0+T_{\text{ref}}} p_i(n) \exp\left(-j\pi\gamma \left(\left(\frac{n}{f_s} - \tau_0 \right)^2 \right.\right.\right. \\ &\qquad \left.\left.\left. - \left(\frac{n}{f_s} - \tau - \beta_i \right)^2 \right) \right) \right| \\ &= \left| \sum_{n=\tau_0}^{\tau_0+T_{\text{ref}}} p_i(n) \exp\left(-j\pi\gamma \left(2(\tau+\beta_i-\tau_0)\frac{n}{f_s} \right.\right.\right. \\ &\qquad \left.\left.\left. + (\tau_0^2 - (\tau+\beta_i)^2) \right) \right) \right| \\ &= \left| \sum_{n=\tau_0}^{\tau_0+T_{\text{ref}}} p_i(n) \exp\left(-j2\pi\gamma\beta_i \frac{n}{f_s} \right) \right. \\ &\qquad \left. \times \exp\left(-j2\pi\gamma(\tau-\tau_0)\frac{n}{f_s} \right) \right| \\ &= \left| \text{FFT}\left(p_i(n) \exp\left(-j2\pi\gamma\beta_i \frac{n}{f_s} \right) \right) \right|. \end{aligned} \tag{25}$$

Equation (25) above indicates that if the low data rate signal $p_i(n)$ of the ith subarray compensates for a frequency deviation $-\gamma\beta_i$, the projection processing is simplified to the customary fast Fourier transform (FFT).

Combined with the phase deviation compensation discussed earlier, digital orthogonal demodulation can also compensate for the frequency deviation by dynamically adjusting the frequency of the two channels of the orthogonal signals. Thus, (15) can be rewritten as

$$\begin{aligned} U_I(n) &= \cos\left(j2\pi(f_L + \gamma\beta_i)\frac{n}{f_s} - f_c\beta_i \right) \\ U_I(n) &= \sin\left(j2\pi(f_L + \gamma\beta_i)\frac{n}{f_s} - f_c\beta_i \right). \end{aligned} \tag{26}$$

After mixing and low-pass filtering, the complex signal $p_i(n) \cdot \exp(-j2\pi\gamma\beta_i(n/f_s))$ is obtained.

In addition, the high-resolution range profile $P_i(\tau)$ is unrelated to the subarray number. FFT processing can be performed after the subarray channel has been synthesized. Hence, if the frequency is compensated for first, (25) yields the conventional signal processing result.

Theoretical derivations can be used to combine the digital orthogonal demodulation and signal preprocessing components. First, the frequency deviation and the phase deviation are compensated by dynamically adjusting the frequency and phase of the two-way local oscillation signal. Second, the subarray data are summed, and FFT processing is completed. Finally, the high-resolution range profile is obtained. The process is diagramed in Fig. 8.

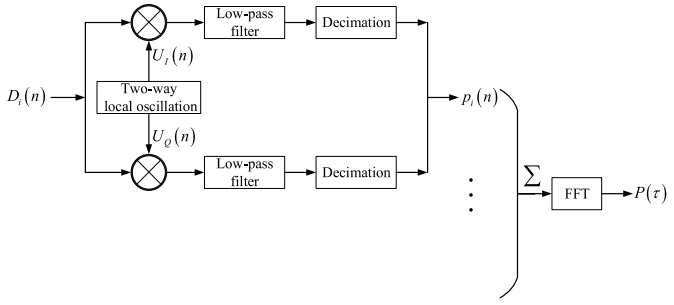

Fig. 8. Diagram of digital orthogonal demodulation and signal preprocessing.

The digital oscillator is obtained via direct frequency synthesis. As shown in Section IV, the resolutions of the signal frequency and phase are determined by the word length N of the PA and the address word length of the sine LUT. The longer the word length, the higher the frequency and phase precision of the orthogonal signal, and the more effective is the compensation effect of the time-delay between the subarray pathways.

C. High-Precision System Synchronization Technology

Compared with analog processing, subarray digital processing places higher requirements on the synchronization of signal generation between multiple subarrays and data acquisition. Accurate synchronization is mainly realized by the strict control of the clock and trigger synchronization in the design of a high-speed multichannel transceiver system.

The time delay between two-channel transceiver clocks produces time-delay errors in the results of the two channels for the same input signal. Thus, the processing results cannot be completely coherent, which decreases the signal-to-noise ratio. In the system design, the phase-locked loop has a good clock skew and jitter index, and a supporting zero-delay clock multiplier is used to provide clocks for multichannel acquisition devices. In addition, the selected acquisition devices support picosecond-level sampling time-delay adjustment, further improving the synchronization performance and simplifying the system design.

When the digital phased array radar is in gate sampling mode, a pulse is needed to trigger and boot data acquisition. If the trigger signals reach the various A/D converters at different times, then multiple channels trigger asynchronization. If the frequency of the sampling clock is very high, the sampling clock is slow relative to the increasing edge of the trigger signal, posing a challenge to the multichannel trigger hold-in range. In the design of trigger synchronization, resampling is used to shape the trigger pulse edge. Thus, the trigger edge becomes steeper, and synchronization is achieved using a high-frequency timing system, thus realizing synchronous coherence at the moment of acquisition.

The coherence of different subarray generation signals and acquisition data can be realized by the refined design of clock and trigger synchronization systems, thus ensuring a phase-coherent synthesis of subarray signals after digital stretch processing.

V. System Integration Verification

To test and verify the function and performance of the proposed architecture, we developed a high-speed digital transceiver unit. Each high-speed digital transceiver unit has the following components: two high-speed A/D paths with an operating clock frequency of 1.6 GSPS and two high-speed D/A paths with an operating clock frequency of 1.6 GSPS for the conversion of analog signals and digital signals; a high-performance FPGA for wideband signal generation, digital stretch processing, and digital modulation; and a DSP for signal preprocessing. The hardware system architecture and the physical product of the high-speed transceiver unit are shown in Fig. 9.

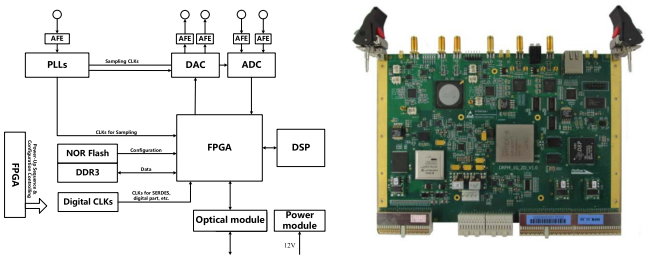

Fig. 9. System architecture and photograph of the high-speed digital transceiver unit.

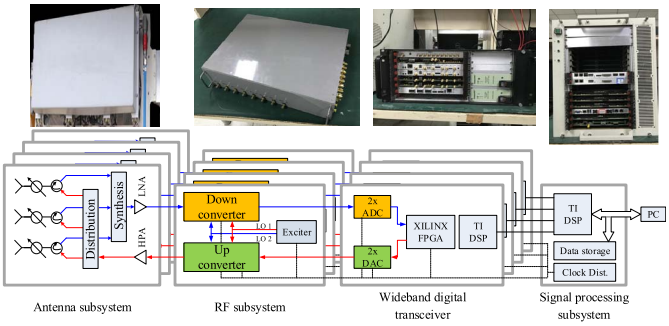

Fig. 10. Schematic of the wideband digital array system.

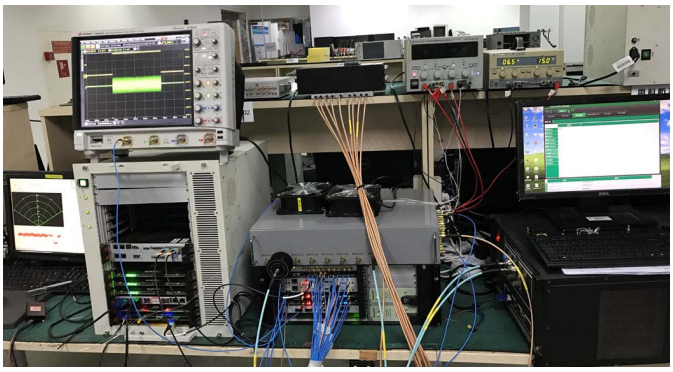

Fig. 11. Photograph of the wideband digital array system.

Based on this, the wideband digital transceiver subsystem is built, which mainly consists of four high-speed digital transceiver units. This subsystem can realize wideband signal transceiver processing of eight subarray paths. The phase consistency index measured between the 1.2-GHz IF signal transmitter paths is less than 2°, and the corresponding time synchronization precision is 4.6 ps. The phase consistency index measured between the 1.2-GHz IF signal receiver paths is less than 4°, and the corresponding time synchronization precision is 9.2 ps.

The wideband digital array radar test system is shown in Figs. 10 and 11. The parameters of the array radar system are shown in Table I.

To meet the acquisition requirements for 600-MHz bandwidth signals, the operating clock frequency of the high-

TABLE I
PARAMETERS OF X-BAND DIGITAL ARRAY RADAR SYSTEM

Parameter	Value
Center frequency	X band
Maximum bandwidth	600 MHz
Sampling rate	25 MHz
Maximum pulse width	0.2 ms
Range window	8 μs
Array size	0.5 m × 0.5 m
Number of subarrays	8

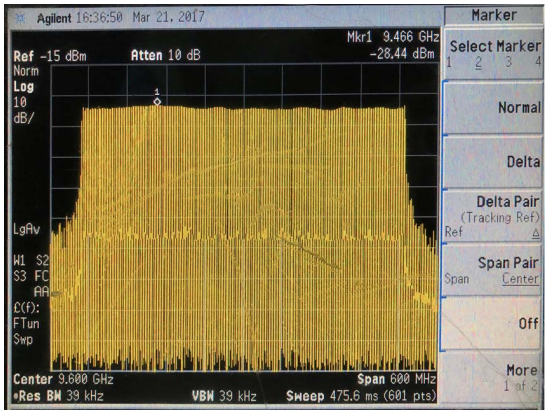

Fig. 12. Spectrogram of 500-MHz LFM signal.

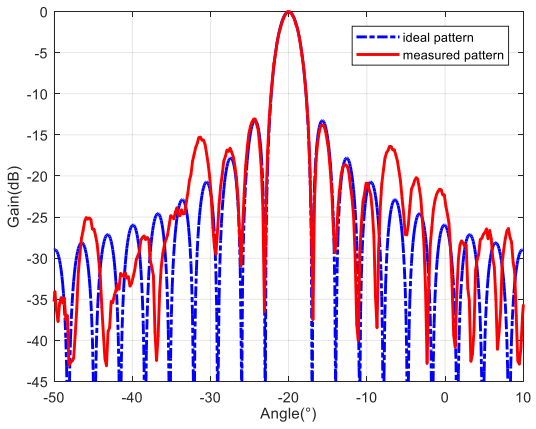

Fig. 13. Digital antenna transmission pattern.

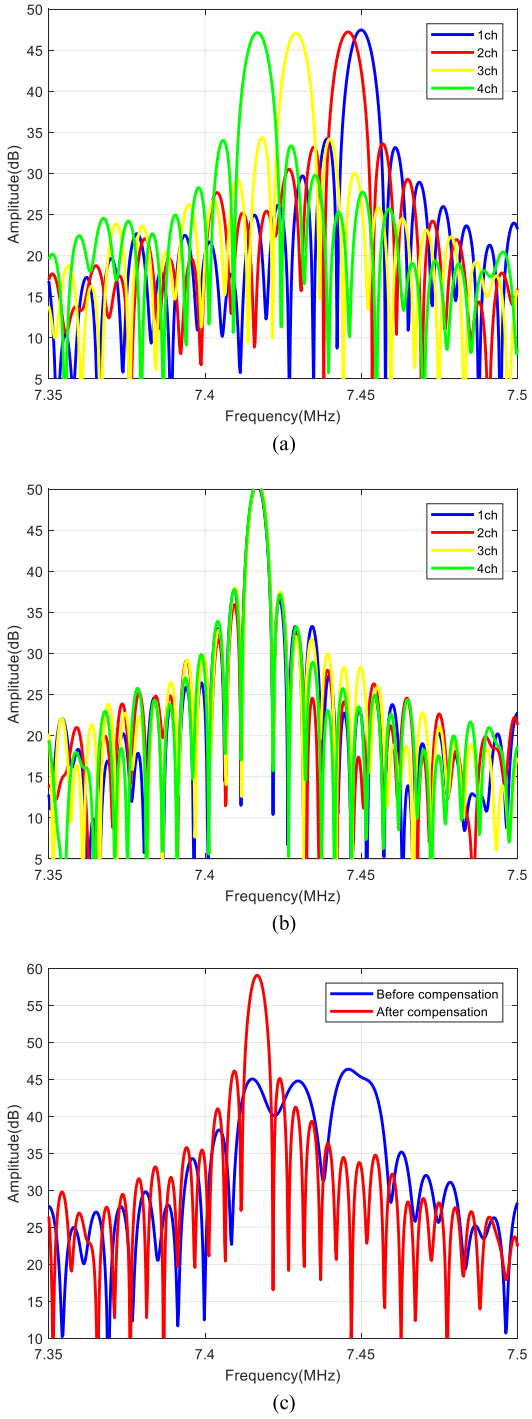

Fig. 14. Subarray digital modulation technique. (a) Before compensation. (b) After compensation. (c) Comparison of synthesis.

speed A/D and D/A converters in the digital transceiver system is set at 1.6 GHz, and the first IF signal is set at 1.2 GHz; thus, the effective range of the bandwidth signal is 1.2 ± 0.3 GHz. The FPGA operating clock frequency is set at 200 MHz; the wideband transmitted signal and the wideband stretched local oscillation signal are generated by eight parallel versatile waveform generators; the word length N of the DDCS accumulator is set at 32, and the word length W of the LUT is set at 16; thus, the frequency resolution of the signal is approximately 0.3725 Hz, and the phase resolution is approximately 0.0055°. The center frequency of the wideband stretched local oscillation signal is set at 1.14 GHz. Therefore, after stretch processing, the second IF signal is set at 60 MHz, and the effective range of the signal is 60 ± 12.5 MHz. After the eight-fold decimation filter, the signal sampling rate is reduced to 200 MHz. Finally, the signal is converted to the baseband upon digital modulation, and the signal sampling rate is reduced to 25 MHz through eight-fold decimation processing.

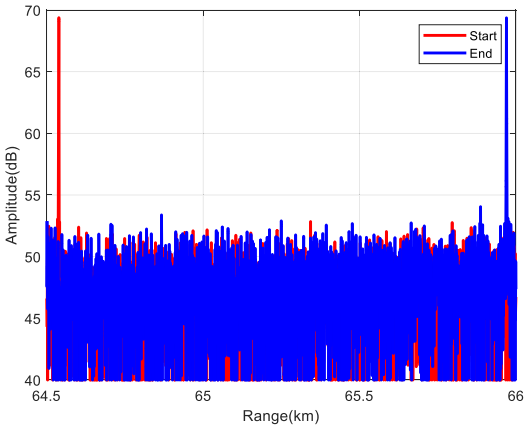

Fig. 15. Range window measurement result.

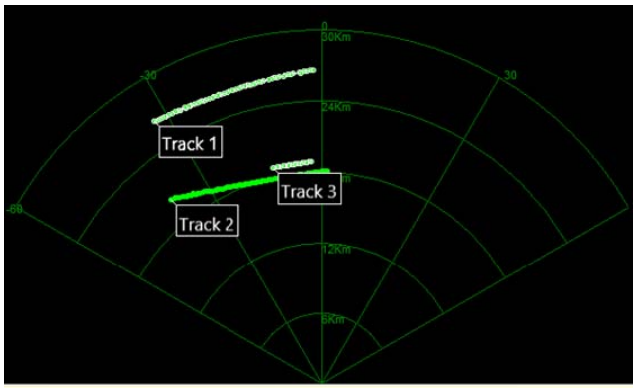

Fig. 16. Real-time tracking of three civil aircraft.

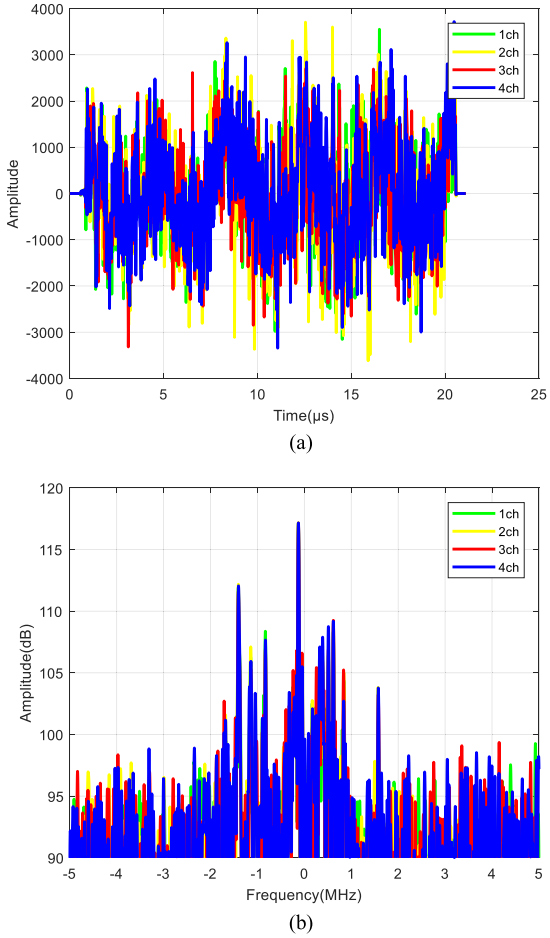

Fig. 17. Echo data of a civil aircraft target. (a) Time domain. (b) Frequency domain.

A. Functional Verification

The functional verification of the system is conducted in an anechoic chamber. The array radar transmits an LFM signal with a bandwidth of 500 MHz and a pulsewidth of 20 μs. The frequency spectrum of the transmitted signal is shown in Fig. 12 (the range of the spectrum analyzer is 600 MHz). The signal bandwidth is demonstrated to be 500 MHz, indicating the feasibility and effectiveness of the wideband waveform generator.

The wideband digital transmitting beamforming technology is verified by drawing an array transmission pattern at a specific angle. The beam pointing is set to $-20°$, and the antenna pattern is shown in Fig. 13, where the dashed line is the ideal antenna pattern, and the solid line is the measured antenna pattern. The main lobe position and width of $-20°$ and 3.6°, respectively, of this pattern are consistent with those of an ideal array antenna pattern. Thus, the transmitted beam is formed by digital modulation.

Four subarray paths are selected to receive the wideband signals transmitted in a specific direction to verify the wideband digital received beam. Fig. 14(a) shows the high-resolution range profile when the dispersion loss is not compensated by digital modulation. The deviation in the peak of the profile of each subarray path will degrade the echo coherence performance. Fig. 14(b) shows the high-resolution range profile after digital modulation, where each subarray path has almost the same peak. Therefore, phase-coherent superposition is realized. Fig. 14(c) shows the superposed result of the four-subarray echo. Without digital modulation processing, the main lobe of the 1-D range profile is expanded four times after superposition. Digital modulation processing effectively superposes the profile and improves the superposition energy of the signals of the four subarrays by approximately 12 dB.

Fig. 15 shows the range window measurement result. For a fixed range window position, the target range measurements are 64.5 and 66 km for the first and last target appearances, respectively. Therefore, the maximum range window of the proposed architecture of approximately 1.5 km in this example is better than that of the traditional architecture of hundreds of meters [20], [21].

B. Measured Data Verification

One set of real data obtained from the wideband digital array radar test system is applied to verify the proposed architecture. The system transmits an LFM signal with a bandwidth of 500 MHz and a pulsewidth of 20 μs for a detection experiment with a civil aircraft target.

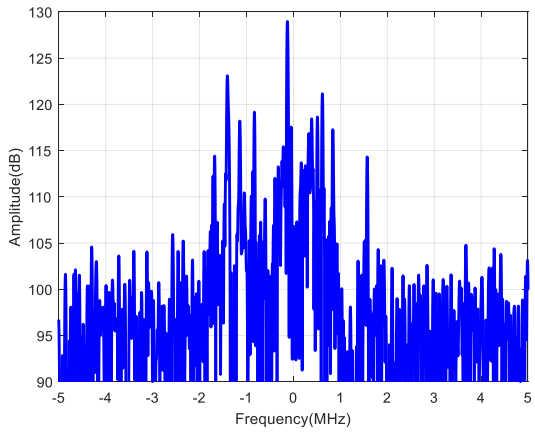

Fig. 18. Target high-resolution 1-D range profile after synthesis of four subarray paths.

Fig. 16 demonstrates the real-time tracking of three civil aircraft. The maximum detection time of the target exceeded 200 s, demonstrating that the aircraft was successfully tracked.

The data of four subarray receiving paths are selected for analysis, and one of the target echoes is shown in Fig. 17.

The frequency-domain diagram shows that the target scattering points of each subarray are aligned, and the phase difference of the strongest scattering point is less than $\pm 5°$. The synthesized high-resolution 1-D range profile is shown in Fig. 18. The echo data of the four paths are effectively superposed after compensation, and the superposition energy of the signals of the four paths is improved by approximately 12 dB.

VI. Conclusion

A novel wideband digital array radar architecture is designed in this article. This system employs digital waveform generation to mitigate signal distortion, digital stretch processing for mass data reduction, high-precision time-delay compensation technology to mitigate dispersion loss, and high-precision system synchronization technology to implement the coherent signal. An engineering implementation scheme is designed, an experimental system is developed, and its performance is evaluated. The wideband digital time-delay compensation method has been validated. The system architecture was shown to have a large measured range window of 1.5 km over a wide instantaneous bandwidth of 500 MHz. This system architecture can support wideband detection tracking and high-precision parameter extraction, as well as digital beamforming.

References

[1] C. Fulton, M. Yeary, D. Thompson, J. Lake, and A. Mitchell, "Digital phased arrays: Challenges and opportunities," *Proc. IEEE*, vol. 104, no. 3, pp. 487–503, Mar. 2016, doi: 10.1109/JPROC.2015.2501804.

[2] S. H. Talisa, K. W. O'Haver, T. M. Comberiate, M. D. Sharp, and O. F. Somerlock, "Benefits of digital phased array radars," *Proc. IEEE*, vol. 104, no. 3, pp. 530–543, Mar. 2016, doi: 10.1109/JPROC.2016.2515842.

[3] D. J. Rabideau, R. J. Galejs, F. G. Willwerth, and D. S. McQueen, "An S-band digital array radar testbed," in *Proc. IEEE Int. Symp. Phased Array Syst. Technol.*, Boston, MA, USA, Oct. 2003, pp. 113–118.

[4] H. Mir, A. Myne, and D. Spinuzzi, "A high dynamic range, wideband digital array radar testbed," in *Proc. Int. Radar Conf.*, Guilin, China, 2009, pp. 1–5.

[5] Y. Wu and J. Li, "The design of digital radar receivers," *IEEE Aerosp. Electron. Syst. Mag.*, vol. 13, no. 1, pp. 35–41, Jan. 1998, doi: 10.1109/62.653823.

[6] Z. Li, L. P. Ligthart, P. Huang, W. Lu, and W. F. van der Zwan, "Trade-off between sensitivity and dynamic range in designing digital radar receivers," in *Proc. Int. Conf. Microw. Millim. Wave Technol.*, Nanjing, China, Apr. 2008, pp. 1368–1371.

[7] Z. Li *et al.*, "Design considerations of the RF front-end for high dynamic range digital radar receivers," in *Proc. 17th Int. Conf. Microw. Radar Wireless Commun. (MIKON)*, Wroclaw, Poland, 2008, pp. 1–4.

[8] O. Adrian, "From AESA radar to digital radar for surface-based applications," in *Proc. IEEE Radar Conf.*, Pasadena, CA, USA, Feb. 2009, pp. 1–5.

[9] P. Lacomme, J. P. Hardange, J. C. Marchais, and E. Normant, *Air and Spaceborne Radar Systems: An Introduction*. Philadelphia, PA, USA: SPIE, 2001.

[10] T. Long, Z. Liang, and Q. Liu, "Advanced technology of high-resolution radar: Target detection, tracking, imaging, and recognition," *Sci. China Inf. Sci.*, vol. 62, no. 4, Apr. 2019, Art. no. 40301, doi: 10.1007/s11432-018-9811-0.

[11] P. Tait, *Introduction to Radar Target Recognition*. Stevenage, U.K.: The Institution of Engineering and Technology, 2005.

[12] D. L. Mensa, "Wideband radar cross section diagnostic measurements," *IEEE Trans. Instrum. Meas.*, vol. IM-33, no. 3, pp. 206–214, Sep. 1984, doi: 10.1109/TIM.1984.4315202.

[13] T. E. Tice, "An overview of radar cross section measurement techniques," *IEEE Trans. Instrum. Meas.*, vol. 39, no. 1, pp. 205–207, Feb. 1990, doi: 10.1109/19.50445.

[14] L. Du, J. Chen, J. Hu, Y. Li, and H. He, "Statistical modeling with label constraint for radar target recognition," *IEEE Trans. Aerosp. Electron. Syst.*, early access, Jul. 5, 2019, doi: 10.1109/TAES.2019.2925472.

[15] A. Aubry, V. Carotenuto, A. De Maio, and L. Pallotta, "High range resolution profile estimation via a cognitive stepped frequency technique," *IEEE Trans. Aerosp. Electron. Syst.*, vol. 55, no. 1, pp. 444–458, Feb. 2019.

[16] W. Caputi, "Stretch: A time-transformation technique," *IEEE Trans. Aerosp. Electron. Syst.*, vols. AES–7, no. 2, pp. 269–278, Mar. 1971, doi: 10.1109/TAES.1971.310366.

[17] H. S. Mir and U. K. Thomas Wong, "Low-rate sampling technique for range-windowed radar/sonar using nonlinear frequency modulation," *IEEE Trans. Aerosp. Electron. Syst.*, vol. 51, no. 3, pp. 1972–1979, Jul. 2015, doi: 10.1109/TAES.2015.130237.

[18] S. S. Haykin, *Adaptive Filter Theory*. Noida, India: Pearson, 2008.

[19] H. Cox, R. M. Zeskind, and M. M. Owen, "Robust adaptive beamforming," *IEEE Trans. Acoust., Speech, Signal Process.*, vol. 35, no. 10, pp. 1365–1376, Oct. 1987.

[20] D. R. Bromaghim and J. P. Perry, "A wideband linear FM ramp generator for the long-range imaging RADAR," *IEEE Trans. Microw. Theory Techn.*, vol. MTT-26, no. 5, pp. 322–325, May 1978.

[21] T. L. Sangiolo and L. B. Spence, "PACS: A processing and control system for the haystack long range imaging radar," in *Proc. IEEE Int. Conf. Radar*, Arlington, VA, USA, Aug. 1990, pp. 480–485.

[22] M. Schikorr, "High range resolution with digital stretch processing," in *Proc. IEEE Radar Conf.*, Rome, Italy, May 2008, pp. 1–6.

[23] Y.-X. Zhang, R.-J. Hong, P.-P. Pan, Z.-M. Deng, and Q.-F. Liu, "Frequency-domain range sidelobe correction in stretch processing for wideband LFM radars," *IEEE Trans. Aerosp. Electron. Syst.*, vol. 53, no. 1, pp. 111–121, Feb. 2017.

[24] M. I. Skolnik, *Radar Handbook*, 3rd ed. New York, NY, USA: McGraw-Hill, 2008.

[25] R. Rotman, M. Tur, and L. Yaron, "True time delay in phased arrays," *Proc. IEEE*, vol. 104, no. 3, pp. 504–518, Mar. 2016, doi: 10.1109/JPROC.2016.2515122.

[26] D. J. Rabideau, "Improved wideband time delay beam-steering," in *Proc. 34th Asilomar Conf. Signals, Syst. Comput.*, Pacific Grove, CA, USA, 2001, pp. 1385–1390.

[27] C. Cheung, R. Shah, and M. Parker, "Time delay digital beamforming for wideband pulsed radar implementation," in *Proc. IEEE Int. Symp. Phased Array Syst. Technol.*, Waltham, MA, USA, Oct. 2013, pp. 448–455.

[28] Y. Yao, X. Huang, G. Wu, and K. Wei, "Joint equalization and fractional delay filter design for wideband digital beamforming," in *Proc. IEEE Radar Conf.*, Arlington, VA, USA, May 2015, pp. 823–827.

[29] W. Fu, D. Jiang, Y. Su, R. Qian, and Y. Gao, "Implementation of wideband digital transmitting beamformer based on LFM waveforms," *IET Signal Process.*, vol. 11, no. 2, pp. 205–212, Apr. 2017, doi: 10.1049/iet-spr.2016.0114.
[30] L. H. Liu Haibo, E. Wang, L. J. Li Jinbing, and R. X. Ren Xiaoyuan, "Rearch on digital compensation technology of wideband phased array radar based on chirp signal," in *Proc. IET Int. Radar Conf.*, Hangzhou, China, 2015, pp. 1–5.
[31] H. S. Mir and L. Albasha, "A low-cost high-performance digital radar test bed," *IEEE Trans. Instrum. Meas.*, vol. 62, no. 1, pp. 221–229, Jan. 2013, doi: 10.1109/TIM.2012.2212497.
[32] Y. Zhang, Q. Bao, J. Wu, and S. Li, "Design and implementation of wideband all digital array radar test-bed," in *Proc. 11th Eur. Radar Conf.*, Rome, Italy, Oct. 2014, pp. 1920–1923.
[33] Y. Jian, Q. Liu, and Q. Luo, "FPGA implementation of digital local oscillator for digital stretch processing," in *Proc. IET Int. Radar Conf.*, Xi'an, China, 2013, pp. 1–4.
[34] M. R. Bales and S. C. Sutphin, "FPGA architecture for real-time wideband waveform synthesis," in *Proc. IEEE Radar Conf. (RadarCon)*, Arlington, VA, USA, May 2015, pp. 605–610.
[35] S. D. Blunt and E. L. Mokole, "Overview of radar waveform diversity," *IEEE Aerosp. Electron. Syst. Mag.*, vol. 31, no. 11, pp. 2–42, Nov. 2016, doi: 10.1109/MAES.2016.160071.
[36] D. M. Hemmingsen *et al.*, "Waveform-diverse stretch processing," in *Proc. IEEE Radar Conf.*, Oklahoma City, OK, USA, Apr. 2018, pp. 0963–0968.

Zhennan Liang was born in Shanxi, China, in 1992. He received the B.S. degree in electronic science and engineering from Southeast University, Nanjing, China, in 2014. He is currently pursuing the Ph.D. degree with the Department of information and Electronics, Beijing Institute of Technology, Beijing, China.

His research interests include digital phased array radar system and wideband radar signal processing.

Quanhua Liu (Senior Member, IEEE) was born in Fujian, China, in 1982. He received the B.S. degree in telecommunications engineering from the Beijing Information Technology Institute, Beijing, China, in 2005, and the Ph.D. degree in target detection and recognition from the Beijing Institute of Technology (BIT), Beijing, in 2010.

From 2010 to 2011, he was a Post-Doctoral Researcher with the Antenna and Microwave Laboratory, The University of Tennessee, Knoxville, TN, USA. Since 2011, he has been a Faculty Member with BIT, where he is currently an Associate Professor. His research interests include wideband radar signal processing and distributed radar systems.

Teng Long (Fellow, IEEE) was born in Fujian, China, in 1968. He received the M.S. and. Ph.D. degrees in electrical engineering from the Beijing Institute of Technology, Beijing, China, in 1991 and 1995, respectively.

He was a Visiting Scholar with Stanford University, Stanford, CA, USA, in 1999, and University College London, London, U.K., in 2002. He has been a Full Professor with the Department of Electrical Engineering, Beijing Institute of Technology, since 2000. His research interests include synthetic aperture radar systems and real-time digital signal processing, with applications to radar and communication systems.